Proceedings of 20th International Congress on Acoustics, ICA 2010

23-27 August 2010, Sydney, Australia

A new model for the shapes of rate-level functions of auditory-nerve fibers

Peter Heil (1), Heinrich Neubauer (1) and Dexter R.F. Irvine (2,3)

(1) Leibniz Institute for Neurobiology, Magdeburg, Germany
(2) School of Psychology and Psychiatry, Monash University, Melbourne, Australia
(3) Bionic Ear Institute, Melbourne, Australia

PACS: 43.64.PG; 43.64.BT

ABSTRACT

All acoustic information relayed to the central nervous system is encoded in the spiking patterns of auditory-nerve (AN) fibres. Here we re-examine and model the dependence of the spike rates of AN fibres on the amplitude of tonal stimuli, building upon the seminal study of Sachs and Abbas (1974). These authors modelled the spike rate vs. sound amplitude functions of AN fibres as the result of the interaction of a 'mechanical stage', describing basilar membrane displacement as a function of sound amplitude, with a 'transducer stage', converting displacement into AN fibre spike rate. The latter stage was modelled as a saturating power function, and spontaneous rate was assumed to simply add to the sound-driven rate. However, the 'transducer stage' of the model – though widely used – has several limitations. Here, we present a physiologically plausible modification of this stage. With this modification, spontaneous activity and its tight correlation with AN fibre sensitivity are emergent properties of the model. Furthermore, we show that for frequencies well below characteristic frequency (CF), where the mechanics are linear, the power which best accounts for all 154 measured cat AN fibre rate-level functions is 3, independent of spontaneous rate or CF. Since this power is the same as that obtained from analysis of absolute thresholds at the perceptual level (Heil and Neubauer, 2003; Neubauer and Heil, 2004), our model also unites AN fibres properties with psychophysics.

INTRODUCTION

The auditory nerve (AN) constitutes the conduit or the flow of acoustic information to the central auditory system. Here we re-investigate the dependence of the spike rates of AN fibres on the amplitude or sound pressure level (SPL) of acoustic stimuli. Comprehensive models of the auditory periphery have been developed which – among other features – produce spike rate versus sound level functions similar to those observed experimentally (e.g. Meddis, 2006; Zhang et al., 2001). However, the sheer number of model components makes it difficult to identify those that are most relevant for producing a particular output, and makes the fine-tuning of model parameters to experimental data impossible. We pursue the alternative of a tractable, parsimonious, yet satisfactory model. Such an approach may also turn out to be valuable for an improved interpretation of the changes in AN rate-level functions consequent on various forms of hearing loss (e.g. Heinz and Young, 2004). We build upon the pioneering and highly influential model of Sachs and Abbas (1974), developed more than 35 years ago. This model consists of a mechanical stage, essentially capturing the basilar membrane (BM) vibration amplitude as a function of the sound amplitude, followed by a saturating non-linearity, termed the 'transducer' stage by Sachs and Abbas. This transducer stage, a saturating power function, describes the spike rate of AN fibres as a function of the BM displacement. This model has been widely used, and provides good fits to empirical rate-level functions in the reptilian, avian, and mammalian species studied (e.g. Winslow and Sachs, 1988; Sachs et al., 1989; Yates, 1990, 1991; Yates et al., 1990, 2000; Eatock et al., 1991; Müller and Robertson, 1991; Müller et al., 1991; Ohlemiller et al., 1991; Winter and Palmer, 1991; Richter et al., 1995; Köppl and Yates, 1999; Nizami, 2002; Saunders et al., 2002; Lütkenhöner, 2008; Wen et al., 2009). Nevertheless, the model has several limitations, which stress the need for a better one. In order to develop an improved model, we first simplify the Sachs-Abbas-model even further by restricting the analysis to AN fibre responses to stimulus frequencies well below the characteristic frequency (frequency at which threshold is lowest; CF), thereby avoiding confounding effects of BM non-linearities resulting from the action of the active process (Robles and Ruggero, 2001; Hudspeth, 2008). In this way, we can focus on the transducer stage in isolation. We then introduce a single, physiologically highly plausible modification which removes the major limitations of the Sachs-Abbas model. Our new model for the transducer stage can, of course, then be combined again with a mechanical stage to account for AN fibre rate-level functions also at and near CF.

The Sachs-Abbas model (Model 1)

When the BM displacement is a linear function of sound amplitude, as is the case for frequencies well below CF, except at very low CFs (Cooper and Rhode, 1992; Robles and Ruggero, 2001), the model of Sachs and Abbas (1974) simplifies to:

$$R(P) = R_d(P) + R_{spont} = \frac{R_{\max d} \cdot P^{\alpha}}{R_{\max d} / k_1 + P^{\alpha}} + R_{spont} \quad (1)$$

In this model, the firing rate $R(P)$ of an AN fibre as a function of the stimulus amplitude P (in Pa) is considered to be the sum of a stimulus-driven rate $R_d(P)$ and a spontaneous rate R_{spont}. R_{maxd} is the maximum driven rate (in s^{-1}), and α a dimensionless power. The parameter k_1 is a measure of sensitivity (in $Pa^{-\alpha} \cdot s^{-1}$). The stimulus amplitude at which the driven rate is equal to half the maximum driven rate is given by $(R_{maxd} / k_1)^{1/\alpha}$. Of course, for a given fibre, k_1 varies with stimulus frequency, while for any given frequency, k_1 will differ among fibres.

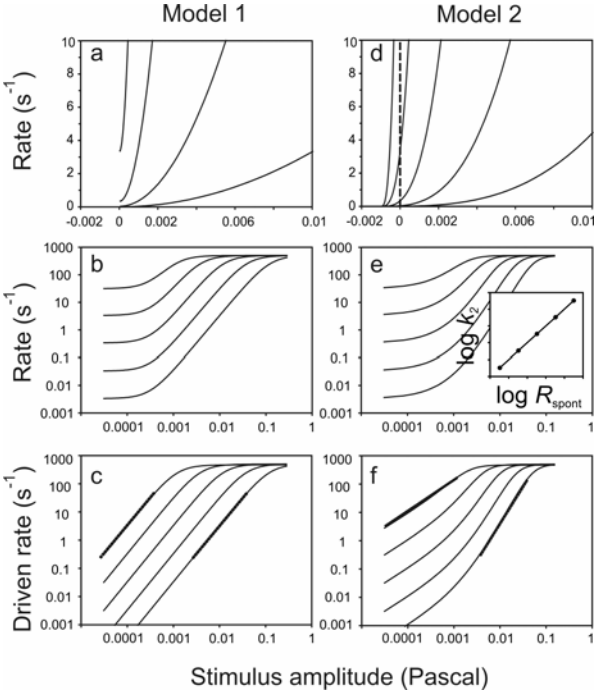

Figure 1. Spike rate versus stimulus amplitude functions generated according to the Sachs-Abbas model (model 1; **a-c**) and according to the model proposed here (model 2; **d-f**). Panels **a** and **d** show a family of functions differing in sensitivity and spontaneous rate and plotted in double-linear coordinates. The functions in **a** were generated with α=2, R_{maxd}=500 spikes/s, and different values of k_1 and R_{spont} which co-varied over 4 orders of magnitude. The functions in **d** were generated with β=3, R_{max}=500 spikes/s, and P_0 = 1 mPa. Only the sensitivity parameter k_2 varied, over 4 orders of magnitude. The vertical dashed line marks P = 0, and the intersections of the rate functions with that line allow the emerging values of R_{spont} to be read off; R_{spont} then co-varies with sensitivity (inset in **e**). Panels **b** and **e** show the same functions (for $P > 0$) in double-logarithmic coordinates, and panels **c** and **f** show the corresponding driven rates, given by $R(P) - R_{spont}$. Thick lines indicate local slopes.

Despite its wide use and the good fits to empirical AN fibre rate-level functions, several caveats can be raised against this model. Here, we mention only two. First, in the model the spontaneous rate and the sensitivity are independent. Hence, the model provides no explanation for the universally observed tight positive correlation between sensitivity (at CF) and spontaneous rate in mammalian AN fibers (e.g. Kiang et al., 1965; Winter et al., 1990; Tsuji and Liberman, 1997; Taberner and Liberman, 2005). To reproduce this tight empirical correlation, k_1 and R_{spont} in equation (1) must be set so that they co-vary. Second, there is disagreement between different studies with respect to the value of the power α. Sachs and Abbas (1974) proposed a value of 1.77, but the most common value now in use is 2, implying that the auditory system is driven by sound intensity (since intensity is proportional to the square of sound amplitude) (e.g., Yates, 1991; Yates et al., 1990, 2000; Müller and Robertson, 1991; Müller et al., 1991; Winter and Palmer, 1991; Richter et al., 1995; Köppl and Yates, 1999; Saunders et al., 2002; Lütkenhöner, 2008). However, it has also been proposed that α may systematically vary between about 1 and 3 with AN fibre spontaneous rate, suggesting that the rate-level functions of fibres with different spontaneous rates may be generated by different mechanisms (Geisler et al., 1985; Geisler, 1990, 1997; Eatock et al., 1991; Nizami, 2002). Figure 1a,b shows a family of rate versus stimulus amplitude functions generated according to this model (1), using a single value of R_{maxd} = 500 spikes/s and a single value of α=2. The sensitivity parameter k_1 varies over 4 orders of magnitude and R_{spont} co-varies over nearly 4 orders of magnitude to mimic the empirical positive correlation between sensitivity and spontaneous rate.

A new model (Model 2)

Here we propose an attractive and physiologically plausible alternative to simply adding R_{spont} to the driven rate. We assume that R_{spont} comes about by a force that acts just like the sound amplitude and that these forces, rather than the firing rates, are additive. In this scenario, the total rate $R(P)$ is given by:

$$R(P) = \frac{R_{\max} \cdot (P + P_0)^{\beta}}{R_{\max} / k_2 + (P + P_0)^{\beta}} \qquad \text{for } P \geq -P_0$$

$$R(P) = 0 \qquad \text{for } P < -P_0 \quad (2)$$

Here, P_0 is the sound-amplitude equivalent baseline or point of operation (also measured in Pa) to which the effects of the sound amplitude P add and which gives rise to the spontaneous activity, R_{max} is the total maximum rate, and β is the power. We use β rather than α, since the powers of the two models are not identical (see below) and to avoid confusion. The sum of the stimulus amplitude and of P_0 at which the total rate is equal to half the maximum rate is given by $(R_{max} / k_2)^{1/\beta}$. Figure 1d,e plots a family of rate versus amplitude functions generated according to model 2, with R_{max} = 500 spikes/s, β=3, and P_0 = 1 mPa. Only the sensitivity parameter k_2 varies, over 4 orders of magnitude. The vertical dashed line marks P = 0, and the intersections of the rate functions with that line allow the resulting values of R_{spont} to be read off; R_{spont} varies over nearly 4 orders of magnitude. In this scenario, therefore, the spontaneous activity is an *emergent* property of the system, which depends on P_0, k_2, and R_{max} and which can be calculated from equation (2) with P = 0. AN fibres are spontaneously active unless P_0 = 0 or unless k_2 = 0. In the latter case, however, they could not be driven by sound either, so this case can be ruled out. If P_0 is the same for a subgroup of fibres, say those that innervate the same inner hair cell and hence have the same CF (as in Fig. 1d), R_{spont} will vary with the fibers' sensitivity to CF tones (or of any other given frequency) according to:

$$R_{spont} \cong P_0^{\beta} \cdot k_2 \quad (3)$$

Hence, in a double-logarithmic plot of R_{spont} versus k_2 data points from such a subgroup should fall on a straight line with a slope of about 1 (inset in Fig. 1e), much like what is seen in real data (e.g. Tsuji and Liberman, 1997; Heil and

Neubauer, 2001; Neubauer and Heil, 2008). In this model, therefore, differences in only a single parameter, viz. k_2, suffice to account for the differences in spontaneous rate among AN fibres (once frequency is factored out) and for the empirical correlation between spontaneous rate and sensitivity, while the Sachs-Abbas model needs two parameters.

Comparison of the two models

The two models can produce similar functions (cf. Figure 1b,e). In the case that $R_{spont} = 0$, models 1 and 2 in fact produce identical functions when $k_1 = k_2$ and $R_{maxd} = R_{max}$. In the case that $\alpha = \beta = 1$, the two models can also yield identical functions for $P \geq -P_0$, when the values of R_{spont} in the two models as well as those of R_{max} are identical, and the others are related by: $\sqrt{k_1 \cdot k_2} = R_{spont} / P_0$ and $\sqrt{k_1 / k_2} = (R_{max} - R_{spont}) / R_{max}$.

METHODS

All surgical and experimental procedures were approved by the Monash University Department of Psychology Animal Ethics Committee. Adult cats (2 females, 2 males; weighing 3-3.5 kg) with clean tympani were anesthetized with pentobarbitone sodium (40 mg/kg i.p.) and prepared for recordings from the left AN, as described in detail elsewhere (Heil and Irvine, 1997; Heil et al., 2007). Anesthesia was maintained throughout the experiments by i.v. injections of pentobarbitone, mixed with physiological saline containing 5% glucose. Acoustic stimuli were digitally produced and presented to the cat's left ear via a calibrated sealed sound delivery system. Once a fiber was encountered and well-isolated, up to 200 repetitions of tones with a given frequency (at CF first) and of 100 ms duration and shaped with brief rise and fall times were presented at 4 s^{-1}, at sound pressure levels (SPLs) increasing from low to high values in small steps (most often 4-dB), followed by recording the fibre's spontaneous activity. If the recording conditions remained stable, a new frequency, most commonly 1, 0.75, or 0.5 octaves below the CF, was selected and the protocol repeated. All spikes falling within a window commencing with tone onset and ending 10 ms after tone offset were used to compute a mean spike rate. The Solver of Excel was used to perform least-squares fit of the model functions to the data using the Newton procedure. The models were fit to the logarithm of the spike rate.

RESULTS

We obtained 154 rate-level functions from 82 AN fibres with CFs from 0.3 kHz to 39.3 kHz, and spontaneous rates from near zero up to more than 100 spikes/s, covering the wide range of spontaneous rates reported in the cat and other mammalian species (e.g., Kiang et al., 1965; Müller and Robertson, 1991; Relkin and Doucet, 1991; Taberner and Liberman, 2005). Each rate-level function was fitted with models 1 and 2, with the parameters α and β free or fixed at specified values and the other 3 parameters free.

Evaluation of model predictions

Model 1 predicts that if R_{spont} is subtracted from the total rate $R(P)$, to yield the stimulus driven rate, the maximum slope of the function relating ($R(P)$ - R_{spont}) to P in double-logarithmic coordinates should be equal to the value of α (Figure 1c). If α were constant across AN fibres, estimates of α derived from fits of model 1 to real data should therefore scatter unsystematically around the true value (Figure 2a). If, however, rate-level functions are generated according to model 2 and with a fixed β (> 1), the maximum slope of the driven rate should decrease systematically with increasing sensitivity and hence with increasing spontaneous rate, as shown in Figure 1f. Estimates of the slope of each function in that panel, say for driven rates from >0.1 to about 100 spikes/s, decrease from just under 3 (the right dotted line has a slope of 3) to about 1 (the left dotted line has slope of 1). Thus, such slope estimates do not return the common power of β used to generate the model functions (β=3 in Figure 1). Instead, they underestimate the power, the more so the higher the spontaneous activity. In other words, if rate-level functions were generated according to model 2 with a fixed value of β (> 1), irrespective of spontaneous rate, but were fitted with the Sachs-Abbas model (model 1) with α as a free parameter, then the estimates of α should decrease systematically with increasing spontaneous rate (Figure 2b). Conversely, if rate-level functions were generated according to the Sachs-Abbas model with a fixed value of α, irrespective of spontaneous rate, but were fitted with our new model (model 2), the resulting estimates of β should increase systematically with increasing spontaneous rate (not shown).

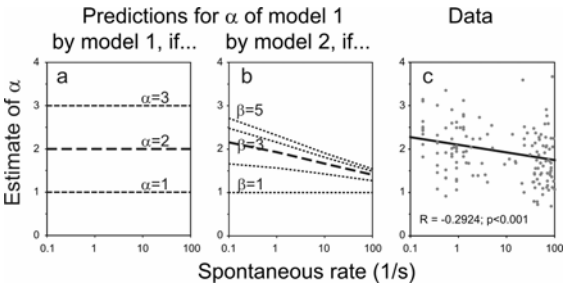

Figure 2. Model predictions for estimates of α of model 1. **a**. If rate-level functions were generated according to model 1 with a single value of α, fits of such functions with model 1 should return estimates of α that are independent of spontaneous rate. **b**. If rate-level functions were generated according to model 2 with a single value of β (> 1), fits of such functions with model 1 should return estimates of α that decrease with increasing spontaneous rate. For β=1, they should be independent of spontaneous rate. **c**. Estimates of α derived from the data decrease significantly with increasing spontaneous rate, a finding that clearly favours model 2.

Figure 2c plots the estimates of α derived from fits of model 1 to the data as a function of spontaneous activity. A few data points derived from records without spontaneous spikes are not shown. Although the estimates of α scatter, there is a clear and highly significant negative relationship between α and the logarithm of the spontaneous rate (R= - 0.2924; n=154; p=0.000234), as predicted by model 2, if β is constant, but not as predicted by model 1, if α is constant. Values of β between 3 and 4 appear to best fit the observed data. Conversely, the correlation coefficient between β and the logarithm of the spontaneous rate was R= 0.0214, which is not significant (p=0.7921), again as predicted by model 2, if β is constant, but not as predicted by model 1, if α is constant. These observations favour model 2 over model 1.

The values of β and α

The 154 estimates of the power β were broadly and asymmetrically distributed (Figure 3a; black circles), yielding a median of 3.83 and an interquartile range of 2.15 to 8.52. However, given the unavoidable noise in recorded AN fibre rate-level functions, the reliability or accuracy with which β can

be estimated depends on the relative range over which $R(P)$ varies with changes in SPL. If the ratio between the maximum rate and the spontaneous rate is small, the estimates of β are less reliable than when that ratio is high. We therefore examined the distributions of the estimates of β separately for rate-level functions with different values of R_{max}/R_{spont}. Figure 3b (black circles and vertical bars) shows that the larger R_{max}/R_{spont}, the narrower is the distribution of estimates, due to a decrease in the upper border without an increase in the lower border. Consequently, the larger R_{max}/R_{spont}, the lower is the median of β. For the largest values of R_{max}/R_{spont}, the estimates of β were narrowly distributed around 3. In contrast, the estimates of α derived from fits of model 1 to the same data were rather narrowly distributed with an interquartile range of 1.44 to 2.34 and a median of 1.95 (Figure 3a; grey triangles), and R_{max}/R_{spont} had little, if any, influence on the width of the distribution (Figure 3b; grey triangles and vertical bars).

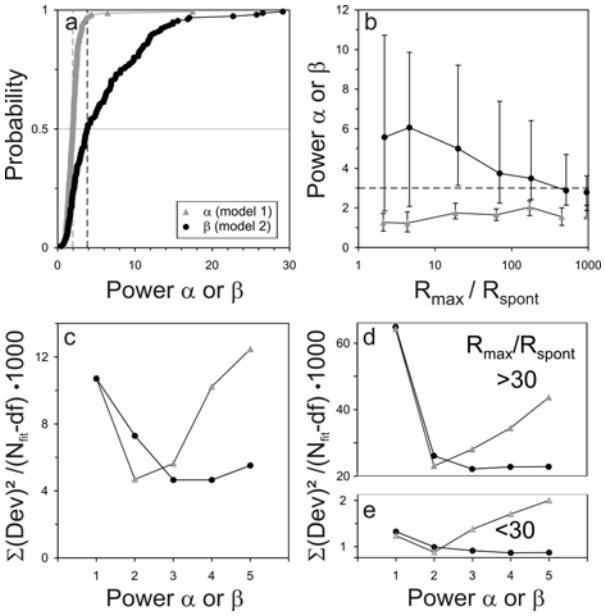

Figure 3. Derivation of the best integer values of β of model 2 and α of model 1. **a**. Cumulative probabilities of estimates of β and α when they are free parameters. The medians (3.83 for β and 1.95 for α) are shown by vertical dashed lines. **b**. Medians and interquartile ranges of the distributions of estimates of β and α calculated separately for functions with similar ratios of R_{max} to R_{spont}. The larger R_{max}/R_{spont}, the narrower is the distribution of β estimates, due to a decrease of the upper, but not the lower, borders of the distributions. For large values of R_{max}/R_{spont}, such as those in Figure 4c, the distribution of β is narrowly centred around 3. For α, there are no such effects. **c-e**. Medians of the summed squared and normalized residuals, calculated across all 154 functions (**c)** or sub-groups with high and low R_{max}/R_{spont} (**d** and **e,** respectively), obtained from fits with models 2 and 1, with β and α fixed at small integer values. Note that errors are smallest for β=3 or 4 (and α=2), but increase asymmetrically, particularly for β. This suggests that, if β is constant and an integer number, it is most likely 3.

We next fitted each rate-level function with model 2, as well as with model 1, fixing β and α to integer values from 1 to 5, and examined the squared residuals. For each function and integer value of the power, we determined the sum of the squared residuals normalized by the difference between the number of data points (in most cases, responses to 20 different SPLs and spontaneous activity were recorded) and the degrees of freedom (df=3). Figure 3c plots the median and the interquartile ranges of this inverse measure of the goodness-of fit across the 154 rate-level functions as a function of β (black circles) and α (grey triangles). For model 2, the best – and about equally good – fits are obtained with values for β of 3 and of 4. Smaller values result in considerably poorer fits, larger values in only marginally poorer fits. Similar results are obtained when the data are examined separately for AN fibres with large and with small values of R_{max}/R_{spont} (Figure 3d,e). The residuals change very little for β > 3, particularly if R_{max}/R_{spont} is small. These asymmetric effects on the residuals of changes in β away from its presumed optimum of 3 (see Figure 3b) are due to an inherent asymmetry in the way a function generated according to model 2 can be approximated by values of β smaller or larger than the one used to generate the function, as explored with simulations (not shown here). In contrast, with model 1 such an asymmetry is less pronounced and the optimal integer value of α across the population of rate-level functions is 2 (Figure 3c-e; grey symbols), confirming previous suggestions (e.g. Müller et al., 1991). In summary, our analyses suggest that the best integer value for the power β of our new model is 3.

Application of model 2 with β=3

Figure 4 shows eight examples of rate-level functions from AN fibres differing widely in spontaneous rate and in CF, along with the fits of model 2 when β is fixed at the presumed best integer value of 3. The quality of the fits is obvious. Across our sample, the fits with model 2 and β=3 were marginally, though not significantly, better than those with the conventional model 1 and α=2 (e.g., cf. the inverse measures of the goodness-of-fit in Figure 3c-e).

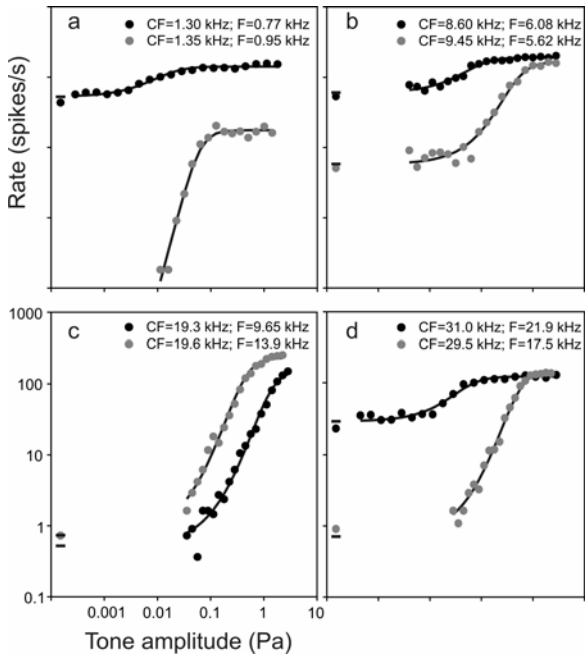

Figure 4. **a-d**. Representative rate-level functions. Circles represent spike rates recorded from 8 different AN fibres of different CFs and spontaneous rates (plotted near the left ordinate). Lines and dashes represent the fits of each data set with model 2 and with β=3. Axes labels in **a** and **c** apply to all panels. CF and stimulus frequency (F) are identified.

The quality of the fits by model 2 and β=3 can be further appreciated by superimposing all individual spike rate measures from the 154 rate-level functions onto the common model function $y = x^3/(1+x^3)$. This requires the normalization and transformation of each individual data set such that $y = R(P)/R_{max}$ and $x = (P+P_0)/((R_{max}/k_2)^{1/3})$. Figure 5 provides such a plot and shows that the 3,065 individual spike rate measures scatter closely and apparently unsystematically around the model function.

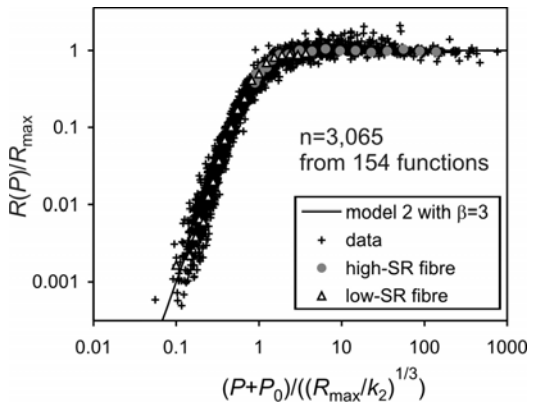

Figure 5. Superimposition of all rate-level combinations (n=3,065) from all 154 rate-level functions onto the model function (model 2 with β=3) using the appropriate transformation. Data points of two functions, one from a high-SR and one from a low-SR fibre, are highlighted. Note the close scatter of the data points around the model.

Parameters of model 2

All 3 free parameters of model 2 (R_{max}, P_0, k_2), and consequently also R_{spont} (cf. equation (3)), varied widely between AN fibres. In 50 of the 82 AN fibres, rate-level functions were obtained at two or more frequencies, all well below CF, allowing an examination of the changes in parameter estimates with stimulus frequency for individual fibres. As expected, for any given AN fibre, estimates of R_{max} and R_{spont} varied little and unsystematically with stimulus frequency (not shown). On the other hand, and with increments in stimulus frequency from 1 to 0.5 octaves below CF, estimates of the sensitivity k_2 increased systematically by about 2 orders of magnitude (corresponding to 80 dB/octave and matching the steepness of conventional tuning curves) (Figure 6a) while those of P_0 decreased systematically by about 2/3 of an order of magnitude (Figure 6b). The two estimates from any given AN fibre are tightly correlated with slopes near -3 in a double-logarithmic plot (Figure 6c).

DISCUSSION

We have proposed here a new formula to describe rate-level functions of AN fibres measured under conditions where the BM mechanics are essentially linear. Our model has the same small number of free parameters, viz. 3, as the conventional and widely used Sachs-Abbas model, and it provides fits of very similar goodness (Figures 3-5). However, our model is superior because it accounts for the observed tight relationship between spontaneous rate and sensitivity of AN fibres by variation of only a single parameter (viz., k_2), while the Sachs-Abbas model requires the tight co-variation of two parameters which in the model itself are unrelated (see equation (1)). In our model, the co-variation of spontaneous rate and sensitivity is an *emergent* property of the model (Figure 1). Furthermore, our model, with a fixed power of β=3, correctly predicts the subtle but systematic co-variation of the estimates of the power α (when free) of the Sachs-Abbas model with spontaneous rate (Figure 2). This co-variation should not occur if rate-level functions were generated according to the Sachs-Abbas model with a constant power α. Several studies have proposed that the power α of the Sachs-Abbas model varies with spontaneous rate, in the same fashion as observed here and predicted by our model with β=3, and have concluded that the rate-level functions of fibres with different spontaneous rates may be generated by different mechanisms (Geisler, 1990; Eatock et al., 1991). Others have proposed different mechanisms in low- versus high-frequency regions of the cochlea (Johnson et al., 2008). With our model, the assumption of different mechanisms is not necessary. All functions can be fitted very well with a single power of β=3 (Figure 5). Hence, our model provides a more parsimonious explanation of the rate-level functions. Of course, our model can be combined with a (non-linear) mechanical input stage, just as the Sachs-Abbas model, to also account for rate-level functions at and close to CF.

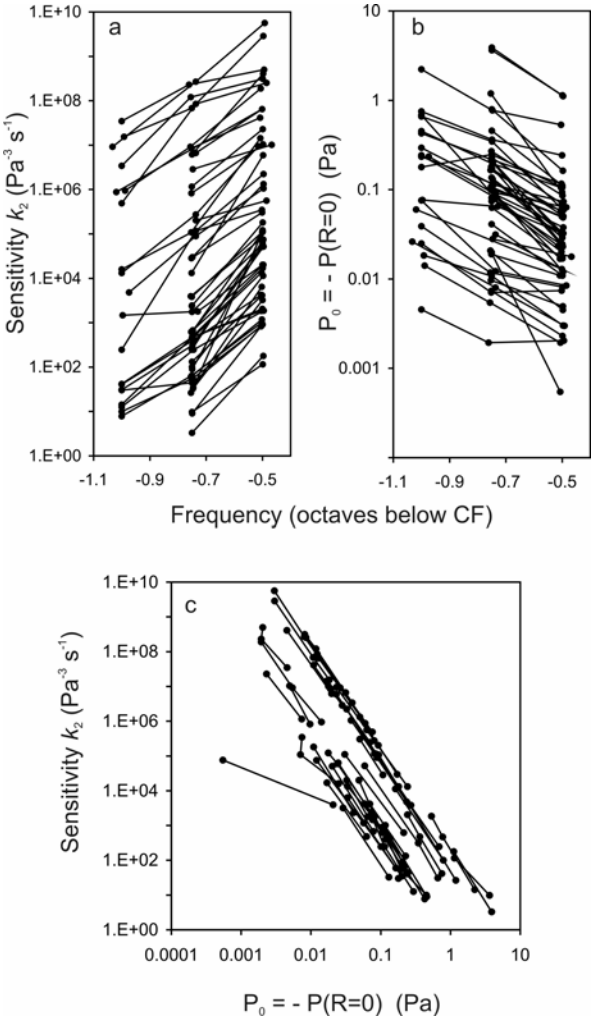

Figure 6. Changes in the estimates of parameters k_2 (**a**) and P_0 (**b**) as a function of frequency and their correlation (**c**). Data from the same AN fibre are connected by straight lines. Note the similar relative increase in k_2 and decrease in P_0 as stimulus frequency approaches CF. Note the tight negative correlation of k_2 and P_0 with a slope of -3 for most data sets in this double-logarithmic plot.

The value of the power β in our new model is clearly larger than 2 and less than 5. Our best estimate of an integer number is β=3 (Figure 3). This value is identical to that derived from fits of a related model developed by us to account for the dependence of the mean first-spike latencies of AN fibres on sound level and rise time (Neubauer and Heil, 2008) and for the distributions of first-spike latencies of low-spontaneous rate fibres on sound level (Heil et al., 2008). Furthermore, a value of 3 (or possibly 4), but not lower, was also derived by us from analyses of a related psychophysical phenomenon, namely the decrease in thresholds (when measured in dB SPL) with increasing stimulus duration at the perceptual level, in a variety of vertebrate species (Heil and Neubauer, 2003; Neubauer and Heil, 2004). Hence, our new model also unites the rate-level functions of AN fibres with this ubiquitous psychophysical phenomenon.

Possible physiological processes underlying the model parameters

What could be the physiological equivalent of P_0 such that it could add to the effects of P? There is strong evidence that in the absence of acoustic stimulation, the membrane potential of the inner hair cell is sufficiently depolarized (around –70 mV) to ensure that the voltage-gated L-type Ca^{2+} channels ($Ca_v1.3$ channels; Brandt et al., 2003; Robertson and Paki, 2002) near the release sites have a non-zero open probability, allowing Ca^{2+} ions to flow into the cell and to trigger transmitter release from synaptic vesicles, which in turn gives rise to spontaneous activity of AN fibres (for review see e.g. Glowatzki et al., 2008). This relatively depolarized membrane potential is maintained by a standing current flowing through the transducer channels near the tips of stereocilia, which in the absence of sound also have non-zero open probability (Wangemann and Schacht, 1996; Kros, 1996). Sound stimulation increases the mean open probability of these transducer channels, depolarizes the membrane potential further, increases the open probability of the $Ca_v1.3$ channels, and hence increases the influx of Ca^{2+} ions needed to trigger release. Therefore, a negative stimulus amplitude of $-P = P_0$ would be required to close all (or nearly all) transducer channels and/or to hyperpolarize the inner hair cell membrane to values sufficient to close all (or nearly all) $Ca_v1.3$ channels, such that transmitter release is prevented. For a given inner hair cell, the negative stimulus amplitude required to achieve these effects will of course be dependent on the cell's sensitivity to the stimulus frequency. Hence, the increase of P_0 as the stimulus frequency moves away from CF (Figure 6b) and the cell's sensitivity decreases (Figure 6a), and the magnitude of the trade-off (Figure 6c), are expected from this interpretation.

In principle, our model can therefore also account for spike rates lower than R_{spont}. With low-frequency tones the instantaneous pressure is negative for half-cycles that are reasonably long relative to the membrane time constant. With such stimuli, it should be possible to validate the prediction of spike rates lower than R_{spont}, and, indeed, instantaneous firing rates below the spontaneous rate, even down to zero, can be observed (e.g., Rose et al., 1967; Palmer and Russell 1986; Palmer and Shackleton 2009). On this view, P_0 defines the point of operation about which $R(P)$ is modulated up or down at low frequencies by positive and negative instantaneous pressures, respectively. Note that since β>1, the increase in $R(P)$ above R_{spont} elicited by a given positive value of P will be larger than the decrease in $R(P)$ below R_{spont} elicited by the same negative value of P. Thus, an expansive power of β=3 will result in, or contribute to, half-wave rectification. Of course, the low-pass filtering properties of the inner hair cell membrane combined with the half-wave rectification will prevent spike rates to fall below R_{spont} in response to high-frequency tones.

The sensitivity parameter k_2 represents a concatenation of all gains in the system up to the level of the recorded AN fibre response. These gains vary among fibres, even for the same stimulus frequency. For any given fibre, the gain also varies with stimulus frequency (Figure 6a). The frequency dependence of k_2 for a given fibre largely reflects the cochlear filtering; the changes in sensitivity (80 dB/octave) over the frequency range studied here (1 to 0.5 octaves below CF) match quite well the steepness of the reported slopes of conventional tuning curves over the corresponding frequency range (e.g. Evans, 1972). Even though it has never been shown directly, it is likely that in mammals AN fibres of different sensitivities and spontaneous rates can innervate the same inner hair cell (e.g. Liberman, 1982). What could account for their differences in sensitivity? Apart from postsynaptic factors, differences in presynaptic factors are likely, as discussed elsewhere (Heil and Neubauer, 2001). Since the inner hair cell is presumably iso-potential, an attractive possibility is that there might be differences in the number or spatial arrangements of the $Ca_v1.3$ channels at the different presynaptic sites. These differences would then lead to differences, at any given membrane potential or change thereof, in the total Ca^{2+} influx and possibly also in the Ca^{2+} concentration near the Ca^{2+} sensors mediating release. Recently, evidence for pronounced differences in the Ca^{2+} influx at different Ca^{2+} hot-spots within the same inner hair cell has been obtained (Frank et al., 2009; Meyer et al., 2009). If our reasoning that the power β=3 represents the binding of 3 Ca^{2+} ions to the Ca^{2+} sensors is correct (see below), 10-fold differences in Ca^{2+} concentration at the different presynaptic active zones would suffice to account for 1000-fold (=10^3; 60 dB) differences in AN fibre sensitivity.

With respect to β, we have argued previously that it might represent the number of Ca^{2+} binding steps to the Ca^{2+} sensors mediating exocytosis from the inner hair cell (Heil and Neubauer, 2003; Neubauer and Heil, 2008; Heil et al., 2008), and this study provides no evidence against this assumption. However, several recent studies have proposed that the Ca^{2+} dependence of vesicle release from inner hair cells were linear (see Glowatzki et al., 2008 for review). Notably, however, most of these studies employed capacitance changes of the inner hair cell membrane and/or whole-cell recordings of Ca^{2+} entry into the cell. Such measures reflect the sum of processes occurring at all of the 10 to 30 synapses of a given inner hair cell and possibly also at extrasynaptic sites. It therefore remains to be seen whether these data can rule out a higher-order Ca^{2+} dependence of vesicle release at individual synapses.

Conclusions

In summary, we have proposed here a new and parsimonious model to account for the shapes of AN fibre rate-level functions. It is a simple saturating higher-order power function, in which the input is the sum of a baseline and of the stimulus amplitude. In this way, the model accounts for spontaneous activity and its tight correlation with AN fibre sensitivity. In addition, a common power of β=3 can account for all experimental data. This suggests that all ribbon synapses in inner hair cells function in essentially the same way, a conclusion also reached by us based on detailed analyses of inter-spike interval distributions during spontaneous activity (Heil et al., 2007). Only differences in sensitivity are needed to account for the variety of the shapes of AN fibre rate-level functions (below CF) and of spontaneous discharge rates.

ACKNOWLEDGEMENTS

We are most grateful to Dr. Mel Brown for his help with the experiments. The study was supported by grants of the Deutsche Forschungsgemeinschaft (DFG) to Peter Heil (He 1721/5-1 and 5-2) and from the National Health and Medical Research Council of Australia to Dexter Irvine for data collection; and from the DFG (SFB-TRR 31 (A6)) to Peter Heil for analysis.

REFERENCES

A. Brandt, J. Striessnig, T. Moser, "$Ca_V1.3$ channels are essential for development and presynaptic activity of cochlear inner hair cells." *J. Neurosci.* **23**, 10832-10840 (2003).

N.P. Cooper and W.S. Rhode, "Basilar membrane mechanics in the hook region of cat and guinea-pig cochleae: Sharp tuning and nonlinearity in the absence of basline position shifts." *Hearing Res.* **63**, 163-190 (1992).

R.A. Eatock, T.F. Weiss, K.L. Otto, "Dependence of discharge rate on sound pressure level in cochlear nerve fibers of the alligator lizard: implications for cochlear mechanisms." *J. Neurophysiol.* **65**, 1580-1597 (1991).

E.F. Evans, "The frequency response and other properties of single fibres of the guinea-pig cochlear nerve." *J. Physiol.* **226**, 263-287 (1972).

T. Frank, D. Khimich, A. Neef, T. Moser, "Mechanisms contributing to synaptic Ca2+ signals and their heterogeneity in hair cells." *Proc. Natl. Acad. Sci. USA* **106,** 4483-4488 (2009).

C.D. Geisler, "Evidence for expansive power functions in the generation of the discharges of 'low- and medium-spontaneous' auditory-nerve fibers." *Hearing Res.* **44**, 1-12 (1990).

C.D. Geisler, "Further results with the 'uniquantal EPSP' hypothesis." *Hearing Res.* **114**, 43-52 (1997).

C.D. Geisler, L. Deng, S.R. Greenberg, "Thresholds for primary auditory fibers using statistically defined criteria." *J. Acoust. Soc. Am.* **77**, 1102-1109 (1985).

E. Glowatzki, L. Grant, P. Fuchs, "Hair cell afferent synapses." *Curr. Opinion Neurobiol.* **18**, 389-395 (2008).

P. Heil P and D.R.F. Irvine, "First-spike timing of auditory-nerve fibers and comparison with auditory cortex." *J. Neurophysiol.* **78**, 2438-2454 (1997).

P. Heil and H. Neubauer, "Temporal integration of sound pressure determines thresholds of auditory-nerve fibers." *J. Neurosci.* **21**, 7404-7415 (2001).

P. Heil and H. Neubauer, "A unifying basis of auditory thresholds based on temporal summation." *Proc. Natl. Acad. Sci. USA* **100**, 6151-6156 (2003).

P. Heil, H. Neubauer, M. Brown, D.R.F. Irvine, "Towards a unifying basis of auditory thresholds: distributions of the first-spike latencies of auditory-nerve fibers." *Hearing Res.* **238**, 25-38 (2008).

P. Heil, H. Neubauer, D.R.F. Irvine, M. Brown, "Spontaneous activity of auditory-nerve fibers: insights into stochastic processes at ribbon synapses." *J. Neurosci.* **27**, 8457-8474 (2007).

M.G. Heinz and E.D. Young, "Response growth with sound level in auditory-nerve fibers after noise-induced hearing loss." *J. Neurophysiol.* **91**, 784-795 (2004).

A.J. Hudspeth, "Making an effort to listen: mechanical amplification in the ear." *Neuron* **59**, 530-545 (2008).

S.L. Johnson, A. Forge, M. Knipper, S. Munkner, W. Marcotti, "Tonotopic variation in the calcium dependence of neurotransmitter release and vesicle pool replenishment at mammalian auditory ribbon synapses." *J. Neurosci.* **28**, 7670-7678 (2008).

N.Y.S. Kiang, T. Watanabe, E.C. Thomas, L.F. Clark, "Discharge patterns of single fibers in the cat's auditory nerve." M.I.T. Research Monograph 35 (1965).

C. Köppl and G.K. Yates, "Coding of sound pressure level in the barn owl's auditory nerve." *J. Neurosci.* **19**, 9674-9686 (1999).

C.J. Kros, "Physiology of mammalian cochlear hair cells." in *The Cochlea* eds. P. Dallos, A.N. Popper, R.R. Fay, (Springer, New York, 1996) pp. 318-385.

M.C.Liberman, "Single-neuron labeling in the cat auditory nerve." *Science* **216**, 1239-1241 (1982).

B. Lütkenhöner, "Threshold and beyond: modelling the intensity dependence of auditory responses." *J. Assoc. Res. Otolaryngol.* **9**, 102-121 (2008).

R. Meddis, "Auditory-nerve first-spike latency and absolute auditory threshold: a computer model." *J. Acoust. Soc. Am.* **119**, 406-417 (2006).

A.C. Meyer, T. Frank, D. Khimich, G. Hoch, D. Riedel, N.M. Chapochnikov, Y.M. Yarin, B. Harke, S.W. Hell, A. Egner, T. Moser, "Tuning of synapse number, structure and function in the cochlea." *Nature Neurosci.* **12**, 444-453 (2009).

M. Müller and D. Robertson, "Shape of rate-versus-level functions of primary auditory nerve fibres: test of the basilar membrane mechanical hypothesis." *Hearing Res.* **57**, 71-78 (1991).

M. Müller, D. Robertson, G.K. Yates, "Rate-versus-level functions of primary auditory nerve fibres: evidence for square-law behaviour of all fibre categories in the guinea-pig." *Hearing Res.* **55**, 50-56 (1991).

H. Neubauer and P. Heil, "Towards a unifying basis of auditory thresholds: the effects of hearing loss on temporal integration reconsidered." *J. Assoc. Res. Otolaryngol.* **5**, 436-458 (2004).

H. Neubauer and P. Heil, "A physiological model for the stimulus dependence of first-spike latency of auditory-nerve fibers." *Brain Res.* **1220**, 208-223 (2008).

L. Nizami, "Estimating auditory neuronal dynamic range using a fitted function." *Hearing Res.* **167**, 13-27 (2002).

K.K. Ohlemiller, S.M. Echteler, J.H. Siegel, "Factors that influence rate-versus-intensity relations in single cochlear nerve fibers of the gerbil." *J. Acoust. Soc. Am.* **90**, 274-287 (1991).

A.R. Palmer and I.J. Russell, "Phase-locking in the cochlear nerve of the guinea-pig and its relation to the receptor potential of inner hair-cells." *Hearing Res.* **24**, 1-15 (1986).

A.R. Palmer and T.M. Shackleton, "Variation in the phase of response to low-frequency pure tones in the guinea pig auditory nerve as functions of stimulus level and frequency." *J. Assoc. Res. Otolaryngol.* **10**, 233-250 (2009).

E.M. Relkin and J.R. Doucet, "Recovery from prior stimulation. I: Relationship to spontaneous firing rates of primary auditory neurons." *Hearing Res.* **55**, 215-222 (1991).

C.P. Richter, S. Heynert, R. Klinke, "Rate-intensity functions of pigeon auditory primary afferents." *Hearing Res.* **83**, 19-25 (1995).

D. Robertson and B. Paki, "Role of L-type Ca2+ channels in transmitter release from mammalian inner hair cells. II. Single-neuron activity." *J. Neurophysiol.* **87**, 2734-2740 (2002).

L. Robles and M.A. Ruggero, "Mechanics of the mammalian cochlea." *Physiol. Rev.* **81**, 1305-1352 (2001).

E. Rose, J.F. Brugge, D. Anderson, E. Hind, "Phase-locked response to low-frequency tones in single auditory nerve fibers of the squirrel monkey." *J. Neurophysiol.* **30**, 769-793 (1967).

M.B. Sachs, P.J. Abbas, "Rate versus level functions for auditory nerve fibers in cats: tone-burst stimuli." *J. Acoust. Soc. Am.* **56**, 1835-1847 (1974).

M.B. Sachs, R.L. Winslow, B.H.A. Sokolowski, "A computational model for rate-level functions from cat auditory-nerve fibers." *Hearing Res.* **41**, 61-70 (1989).

J.C. Saunders, C.E. Ventetuolo, S.K.R. Plontke, B.A. Weiss, "Coding of sound intensity in the chick cochlear nerve." *J. Neurophysiol.* **88**, 2887-2898 (2002).

A.M. Taberner and M.C. Liberman, "Response properties of single auditory nerve fibers in the mouse." *J. Neurophysiol.* **93**, 557–569 (2005).

J. Tsuji and M.C. Liberman, "Intracellular labeling of auditory nerve fibers in guinea pig: central and peripheral projections." *J. Comp. Neurol.* **381**, 188-202 (1997).

P. Wangemann and J. Schacht, "Homeostatic mechanisms in the cochlea." in *The Cochlea* eds. P. Dallos, A.N. Popper, R.R. Fay, (Springer, New York, 1996) pp. 131-185.

B. Wen, G.I. Wang, I. Dean, B. Delgutte, "Dynamic range adaptation to sound level statistics in the auditory nerve." *J. Neurosci.* **29**, 13797-13808 (2009).

R.L. Winslow and M.B. Sachs, "Single-tone intensity discrimination based on auditory-nerve rate responses in backgrounds of quiet, noise, and with stimulation of the crossed olivocochlear bundle." *Hearing Res.* **35**, 165-190 (1988).

I.M. Winter and A.R. Palmer, "Intensity coding in low-frequency auditory-nerve fibers of the guinea-pig." *J. Acoust. Soc. Am.* **90**, 1958-1967 (1991).

I.M. Winter, D. Robertson, G.K. Yates, "Diversity of characteristic frequency rate-intensity functions in guinea pig auditory nerve fibres." *Hearing Res.* **45**, 191-202 (1990).

G.K. Yates, "Basilar membrane nonlinearity and its influence on auditory nerve rate-intensity functions." *Hearing Res.* **50**, 145-162 (1990).

G.K. Yates, "Auditory-nerve spontaneous rates vary predictably with threshold." *Hearing Res.* **57**, 57-62 (1991).

G.K. Yates, G.A. Manley, C. Köppl. "Rate-intensity functions in the emu auditory nerve." *J. Acoust. Soc. Am.* **107**, 2143-2154 (2000).

G.K. Yates, I.M. Winter, D. Robertson, "Basilar membrane nonlinearity determines auditory nerve rate-intensity functions and cochlear dynamic range." *Hearing Res.* **45**, 203-220 (1990).

X. Zhang, M.G. Heinz, I.C. Bruce, L.H. Carney, "A phenomenological model for the responses of auditory-nerve fibers: I. Nonlinear tuning with compression and suppression. *J. Acoust. Soc. Am.* **109**, 648-670 (2001).